NASICON-type $Na_3V_2(PO_4)_3$ as a new positive electrode material for rechargeable aluminium battery

Francisco Nacimiento, Marta Cabello, Ricardo Alcántara*, Pedro Lavela, José L. Tirado

Laboratorio de Química Inorgánica
Instituto de Química Fina y Nanoquímica
Universidad de Córdoba
Campus Universitario de Rabanales
14014 Córdoba, Spain
*E-mail address: ralcantara@uco.es

ABSTRACT

Although rechargeable aluminium-ion batteries could be very promising, there are only a few materials described in the literature that can insert aluminium. NASICON-type $Na_3V_2(PO_4)_3$ (NVP) is here investigated as a new positive electrode, using aluminium chloride dissolved in O_2-free water as electrolyte solution. The reversible capacity is around 60-100 mAh g^{-1}, depending on the cycling conditions. The electrochemical, analytical, NMR, XPS and XRD results all together corroborate that sodium is deinserted during first charge and then aluminium is inserted during the discharge. Both bulk insertion and surface capacitance can contribute to the specific capacity. This is the first report about true insertion of a trivalent cation into a NASICON-type structure. In addition, this material is also electrochemicaly active vs. Al metal in non-aqueous cell, using ionic liquid as electrolyte solution, with a revesible capacity about 60-70 mAh g^{-1} at ca. 1.25 V vs. Al. However, in the case of using ionic liquid, sodium (and not aluminium) is reversibly (de)inserted [23]. The results demonstrate that NVP is promising as electrode for rechargeable aluminium batteries, and that the electrolyte solution strongly influence on the electrochemical reaction.

Keywords: alumninium batteries; NASICON, aqueous batteries; ionic liquid

1. Introduction

Lithium rechargeable battery has been commercialized since the 1990s and is one of the most successful technologies for energy storage, though a post-lithium era is being envisaged.[1] Thus, multivalent metals as aluminium can deliver higher volumetric capacity than Li and are advantageous for large-scale energy storage [1-7]. The high natural abundance, low cost and high volumetric capacity (8040 mAh cm^{-3}) are the main advantages of aluminium. However, to find suitable electrode materials and electrolyte solutions is a great challenge, and the rechargeable aluminium battery is still in its infancy. The main electrode materials proposed in the literature for rechargeable aluminium batteries are vanadium oxides [3,8-11], titanium dioxide [12] sulphides [13], organic polymers [14], Prussian blue analogues [15] and graphite [16-18].

The NASICON-type structure is very useful for providing a stable and open framework that can serve as a host for the insertion of cations. Thus, $A_3V_2(PO_4)_3$ (with A=Li, Na) have been extensively tested as electrode materials for diverse types of rechargeable batteries, particularly lithium, sodium and zinc batteries [19-22]. Very recently, a hybrid Na-Al cell using an ionic liquid containing $NaAlCl_4$ as electrolyte was reported, in which sodium (not aluminium) was reversibly (de)inserted in $Na_3V_2(PO_4)_3$ (NVP) [23]. Nevertheless, the choice of the electrolyte solution can have a strong influence on the (de)insertion process and electrochemical behaviour.

Aqueous ion batteries can be safe, low-cost and environment-friendly [24]. In addition, aqueous electrolytes can exhibit high ionic conductivity and, consequently, deliver high-charge/discharge rates. Nevertheless, the stability of the electrode active material in water limits their development. Besides, aqueous cells can serve as a proof of ion insertion in the meantime that other non-aqueous electrolyte compatible with Al are developed [12]. Sodium vanadium phosphates have been widely investigated as positive electrode in aqueous sodium-ion batteries [25-29], although it has been suggested that NVP degrades upon cycling in aqueous batteries. In

comparison with lithium and potassium, it seems that the insertion of sodium in NVP is easier [25]. The use of NVP/C nanocomposites improves the cycling stability because the carbon phase enhances the electrical conductivity and slows down the dissolution of NVP [26]. Zhou et al. suggested that, on the contrary to Li-Mn-O spinels, NVP cannot support physical adsorption of water through its channels and water cannot interfere with sodium insertion/deintercalation during electrochemical cycling [26]. An aqueous rechargeable battery based on NVP vs. Zn has also been reported [27,30-33].

In this work, the electrochemical insertion of aluminium ions into NVP from aqueous solution is studied, and the mechanism is explored by using XRD, SEM-EDS, XPS and NMR. In addition, the electrochemical behaviour in non aqueous batteries is also studied using ionic liquid as electrolyte solution.

2. Experimental

NVP containing carbon to improve the conductivity was prepared by using a wet ball-milling method, as described elsewhere [34]. For this purpose, firstly ammonium metavanadate (Panreac, 98 %; 1.2 g), sodium dihydrogen phosphate (Aldrich, 98–102 %, 2.1 g), and citric acid (Aldrich, 99 %; 2.9 g) at Na:V:P=2:3:3 molar ratios were added to an agate vessel. Then, 10 mL of ethanol were added to the mixture and the resulting slurry was ball-milled at 300 rpm for 24 h in air. After drying the slurry in an oven at 70°C overnight, a solid precursor was obtained. The final product was prepared by annealing the precursor at 800 °C for 8 h in an argon atmosphere. The presence of the carbon residue (7.3 % wt.) was determined precisely with an Elemental CHNS Eurovector EA 3000 analyzer.

The crystal structure was studied by X-ray diffraction (XRD) using a Bruker D8 instrument with Cu Kα radiation. Rietveld refinement was performed with the TOPAS 4.2 program. The crystal structures were drawn with the VESTA 3.4.0 program [35].

FE-SEM images were obtained using a JSM-7800F Prime instrument. The chemical composition of the electrodes was analyzed by Electron Probe Microanalysis (EPMA) with Energy Dispersive Spectrometer (EDS) detector coupled to FE-SEM.

^{27}Al MAS NMR spectra were acquired at room temperature in a Bruker Avance III HD 400 WB instrument at 12 kHz of spin rate. The chemical shifts were referenced to 1 M aluminium chloride solution (0 ppm). The chemical state of the surface was studied by X-ray Photoelectron Spectrocopy (XPS) in a SPECS Phobios 150 MCD provided with Mg κα source.

All the electrochemical tests were performed in three-electrode cell and using a VMP Biologic instrument. For aqueous batteries, flooded beaker cells were used. The electrolyte solution was 0.1 M $AlCl_3$ in deionized water, the reference electrode was Ag/AgCl and the counterelectrode was Pt. For control experiments, aqueous solutions of HCl and 0.1 M NaCl/HCl at the same pH value (3.0). The working electrode was prepared by mixing the active material (80 %) with carbon black (10 %) and PVDF (10 %) as binder. The aqueous solution was outgassed to remove dissolved oxygen by flowing Ar before carrying out, and during, the electrochemical experiment.

For non-aqueous cell, chloroaluminate ionic liquid was used as electrolyte. This ionic liquid was prepared in the dry box under Ar atmosphere by dissolving anhydrous $AlCl_3$ (99.999% purity, Sigma Aldrich) in 1-ethyl-3-methylimidazolium chloride (EMIC) in molar ratio $AlCl_3$:EMIC=1.1:1.0. The Swagelok-type electrochemical cells comprise three glassy carbon rods (Goodfellow) as current-collectors, a disc of high-purity Al (Aldrich) as reference electrode, another piece of Al as counterelectrode and a working electrode. To prepare the working electrode, the active material (NVP) was mixed with PFTE (binder) and carbon black, and the mixture was pasted on a Pt disc. The use of metals and steel corrodible in ionic liquid was avoided. Whatman glass fiber filter papers were used as separators. The cells were assembled in an M-Braun glove-box filled with Ar.

3. Results and discussion

3.1. Electrochemistry in aqueous cell

The cyclic voltammograms (CV) performed at 1 mV/s are displayed in Fig. 1a. The cut-off voltage was imposed to study the main redox reaction, to achieve approximately the same charge/discharge capacity in all the experiments and to avoid side-reactions, and so it was not fixed. The operating voltage is within the stability window of water. A redox peak is observed at ca. +0.6 for the anodic scan and at ca. +0.2 V for the cathodic scan, although the exact position changes with the cycle number and other experimental conditions. This peak is ascribed to the V^{3+}/V^{4+} redox couple and reversible insertion. In contrast with the observed faradic peak, a pure capacitor behaviour would exhibit intensity-voltage curves with typical rectangular shape, as was found for example in the case of V_2O_5 in KCl aqueous solution [36]. Song et al. proposed that the surface capacitance plays a key role for NVP in aqueous sodium-ion batteries and that the electrochemical reaction is diffusion-controlled [25]. On the other hand, larger size ions as K^+ are preferentially adsorbed on the surface of NVP, rather than inserted into the lattice. Figure 1b shows the CV profiles using 0.1 M NaCl/HCl or HCl as electrolyte solutions at pH 3.0. By comparison, it can be concluded that the CV in $AlCl_3$ solution cannot be ascribed exclusively to sodium and/or protons (de)insertion. In fact, the faradic electrochemical behaviour is better in $AlCl_3$ solution. We can conclude that aluminium is playing a main role in the electrochemistry of NVP.

The separation between the anodic and cathodic peaks is larger at higher rates and the peak current becomes smaller when the scan rate decreases (Fig. 1c). The dependence of the CV with the scan rates (Fig. 1c,d) can be understood on the basis of diffusion and/or capacitive processes. According to the Randles-Sevcik equation, a linear relationship between the intensity of the peak current and the square root of the scan rate is followed when the redox reaction is controlled by diffusion [25,37]. In contrast, a capacitive behaviour normally follows a linear dependence between the current and the scan rate. Thus, in

general, the relationship between the peak current (i) and the scan rate (v) is given by the power law [31,37]:

$$i = av^b \quad (1)$$

where *a* and *b* are adjustable parameters. The value of *b* can be obtained from the slope of the linear fitting of the experimental results on a log-log scale (Figure 1d), and one can expect the current to be dominated by capacitive behaviour at b=1.0, while the current would be dominated by diffusion at b=0.5. This procedure must be taken with caution because capacitive currents can arise from the unavoidable reorganization of the Helmholtz layer at the electrode surface when the potential is swept linearly [37]. Thus, the result is valid within the range of scan rate that is taken (between 5 and 0.3 mV s^{-1} in Figure 1d). The value calculated from the slope of the plot obtained from the oxidation process of the first sweep is *b*=0.67, and in the reduction process of the first sweep *b*=0.70. These *b*-values are intermediate between a purely capacitive behaviour and a diffusion-controlled process. This result implies that at high rate the particle surface would be used for charge storage rather than insertion/deinsertion into the bulk. At high rate, the slow diffusion of the ions limits the insertion/deinsertion process to the outer surface of the NVP particles. Li et al found a value of *b*=0.58 for zinc in NVP, indicating a diffusion-dominated process (not pseudocapacitive) [31]. These results compared to the literature suggest that aluminium diffusion in NVP is slower than that of zinc [32]. It is worth to note here that He et al. found that both bulk insertion (slower process) and surface storage (faster process) contribute to aluminium storage in black anatase TiO_2, although the b-value was not reported in that case [12]. In fact, the coexistence of the two mechanisms (bulk insertion and surface capacitance) in the same electrode material can be beneficial for its electrochemical performance.

In the galvanostatic experiment (Fig. 2) the results agree well with the CV. The profile and capacity of the first charge are different compared with the second and successive charges, in good agreement with irreversible sodium deinsertion. The reversible capacity values in aluminium-ion aqueous batteries are

around 60-100 mAh g^{-1}, depending on the cycling conditions. These capacity values are comparable with the results reported for NVP in non-aqueous sodium-ion batteries [20], and better than the results reported for aqueous sodium-ion batteries (typically around 50-80 mAh g^{-1}) [26,29]. The capacity fade upon further cycling, particularly at slow kinetics, can be due to partial cathode dissolution in the acidic electrolyte as was found in other aqueous batteries, or to structure degradation due to the electrochemical insertion. Perhaps, in future works the resistance of NVP against corrosion could be improved for example by using additives.

3.2. Reaction mechanism and insertion

During the first charge, sodium is removed from NVP. Consequently, some sodium ions are incorporated to the electrolyte solution and a sodium-aluminium hybrid electrolyte is *in-situ* formed, though the relative amount of aluminium ions must be much higher than for sodium ions taking into account the large volume of the flooded cell. The removal of 2 Na per formula is equivalent to 117 mAh g^{-1}, which is the theoretical maximum charge capacity that can be reported in non-aqueous sodium cell and it corresponds to the following reaction:

$$Na_3V_2(PO_4)_3 \rightarrow 2Na^+ + 2e^- + NaV_2(PO_4)_3 \qquad (2)$$

According to previous studies in non-aqueous sodium cell, it is expected that one sodium ion of $NaV_2(PO_4)_3$ remains immobilized at the 6b site and two sodium ions at the 18e site could be extracted [38]. Other authors suggested that sodium can be removed from both sites [39]. The sodium that remains inactive serves as structure Stabilizer. Other reports remarked that water decomposition and O_2 evolution can take place when up to two sodium ions per NVP formula are utilized in aqueous electrolyte [32]. Consequently, we limited the maximum charge capacity up to the nominal composition $Na_{1.1}V_2(PO_4)_3$, irrespectively of the voltage limit. The experimental results of the semiquantitative microanalysis (EPMA-type) coupled to SEM agree quite well with this theoretical composition (Table 1), although traces of electrolyte are detected at the electrode surface.

During the subsequent reduction process, aluminium ions are inserted into partially desodiated NVP, and an aluminated (ANVP) material is formed according to the following reversible reaction:

$$Na_{1.1}V_2(PO_4)_3 + x\ Al^{3+} + 3\ xe^- \rightleftharpoons Al_xNa_{1.1}V_2(PO_4)_3 \qquad (3)$$

According to the microanalysis results, the composition of ANVP electrode retrieved from the cell after the first charge-discharge cycle, and washing the electrode with deionized water, is $Al_{0.25}Na_{0.81}V_2(PO_4)_{2.6}$ (Table 1). Taking into account the theoretical composition ($Al_{0.3}Na_{1.1}V_2(PO_4)_3$) obtained by assuming that all the electrons that flow through the circuit in the reduction process are used for aluminium insertion, the experimental result is in good agreement with aluminium insertion (or surface accommodation). The intrinsic error in the technique (typically higher than 5%), side reactions and traces of electrolyte can contribute to the slight difference between the theoretical and experimental compositions. Besides, the mapping of composition shows that the distribution of aluminium in NVP is homogeneous (Fig. 3). Nevertheless, we cannot completely discard some protons cointercalation together aluminium.

The ^{27}Al NMR spectrum of the electrode after one charge-discharge cycle (Fig. 4a) is in excellent agreement with both insertion and surface accommodation of aluminium. It is worth recalling here that Zhou et al. pointed out that the cross section of the channel in NVP is smaller than the diameter of the water molecule, and inserted aluminium must not be hydrated, and we agree with that find [26]. The spectrum of $Al_{0.3}Na_{1.2}V_2(PO_4)_3$ was fitted with two Gaussian/Lorentzian peaks centered at +37 and – 7 ppm, respectively. The broadening of the peaks can be due to the low mobility of aluminium. The peak at -7 ppm (44% contribution) can be due to aluminium near the surface of NVP particles, while the peak shift due to +37 ppm (56% contribution) can be ascribed to aluminium inserted into the NASICON-type framework. He et al. found smaller shifts for aluminium inserted into anatase, irrespectively of their finding of aluminium accommodation near the surface of anatase particles.[12] For the sake of comparison in a reference measurement, the spectrum of a non-cycled electrode NVP which was simply impregnated

overnight with the electrolyte solution (Fig. 4b) only shows an asymmetric peak at -1.4 ppm and the corresponding spinning side bands. This shift to +37 ppm of the electrode with nominal composition $Al_{0.3}Na_{1.2}V_2(PO_4)_3$ must be due to the effect of the vanadium 3*d* electrons (Fig. 4a). Thus, this result is a very strong proof of veritable insertion of aluminium ion (peak at + 37 ppm), together with aluminium placed near the particle surface (peak at -7 ppm). Similarly, other authors also used ^{27}Al NMR results as a main proof of aluminium intercalation in other materials [12,18].

Although XPS only delivers information about the surface of the particles, it can be useful to follow the electrochemical reactions. The V 2p spectra of raw NVP show two bands at 523.2 and 516.9 eV, which can be attributed to the V $2p_{3/2}$ and V $2p_{1/2}$ transitions, respectively (Fig. 5). These binding energy values are ascribed to V^{3+} [40]. The minor contribution at ca. 520.5 eV corresponds to the O 1s satellite peak. After the charge, the shift of the V 2p bands to higher energies unambiguously demonstrates the partial oxidation of vanadium. During subsequent discharge, the bands are shifted back to values close to those of raw NVP. Irrespectively of the fact that the surface of the charged electrode unavoidably can contain traces of aluminium from the electrolyte, it is evident that in the discharged electrode the relative intensity of the Al 2p band at ca. 75 eV grows, in good agreement with aluminium insertion into NVP. From the relative intensity of the Na 1s band in the spectra, it is deduced that part of sodium is irreversibly removed from NVP. The broadening of the Na 1s band could be due to the presence of sodium in sites with different ionic character and/or near defects. In addition, the ionic character of the sodium-oxygen bond could be affected by the intercalation of aluminium. Thus, the stronger bond aluminium-oxygen can weaker the sodium-oxygen bond.

To study the structural changes occurring in the electrode material during the charge/discharge reaction, we carried out *ex-situ* XRD experiments of NVP in aqueous aluminium cells (Fig. 6). The XRD pattern of the as-prepared NVP sample (Fig. 6) can be indexed on the space group R-3c group. From Rietveld refinement, the resulting lattice parameters are: a=8.735(5) Å, c=21.82(1) Å and V= 1442(2) $Å^3$.

It is worth to remember that partial deintercalation of sodium from NVP does not drive to any drastic change of its structure, and that there is little contrast between sodium and aluminium. Nevertheless, if one takes into account the results of electrochemistry, XPS, microanalyis and NMR, it seems reasonable to deal the XRD results considering aluminium intercalation. After the first partial charge in aqueous solution up to the nominal composition $Na_{1.4}V_2(PO_4)_3$ the observed reflections can be also indexed in the same space group. At the end of the first charge up to the nominal composition $Na_{1.1}V_2(PO_4)_3$, the XRD pattern can be indexed using the same space group, but the shrinkage of the unit cell is more significant (a=8.401(1) Å, c=21.444(7) Å, vol.=1310.8(6) $Å^3$), as expected after regarding the shift of the reflections to higher angles. Also, the splitting of the (104)/(110) peak is observed. Thus, the coexistence of two phases with compositions $Na_3V_2(PO_4)_3$ and ca. $Na_{1.1}V_2(PO_4)_3$ can be the reason of the charge plateau, in good agreement with the literature on sodium batteries. When $Na_3V_2(PO_4)_3$ is oxidized, sodium is partially removed from the 18e sites, and then only 6b sites would be occupied in the phase $NaV_2(PO_4)_3$, although some sodium atoms initially placed at 18e sites may migrate to 6b sites. According to our Rietveld refinement results, most of sodium is placed at 6b sites while only a small amount of sodium remains at 18e sites. After the first charge (up to $NaV_2(PO_4)_3$) and then full discharge down to -0.5 V, the reflections tend to become more broadened due to the lattice strain, and the cell is slightly expanded in the a-axis (a=8.51(1) Å, c=21.81(3) Å, vol.=1368(4) $Å^3$) as compared to the charged material. In comparison with pristine NVP before electrochemical cycling, the unit cell after the first charge-discharge cycle is contracted particularly in the a-b plane, in good agreement with the replacement of sodium by smaller and more polarizing aluminium. Due to the large charge/radius ratio of Al^{3+} and to the attraction between aluminium and oxygen, the diameter of the channel is decreased from 2.723 to 2.676 Å (oxygen-oxygen distance measured in the a-direction). To compensate this contraction, the distance Na1-O2 in the 6b site is expanded from 2.51 to 2.67 Å. This implies that the formation of Al-O bonds weakens the Na-O bonds. The strain of the NASICON-type structure can be the reason of capacity loss upon electrochemical

cycling. The Rietveld refinement, in which the occupancy factor of sodium and aluminium sites was independently liberated, is in good agreement with the occupancy of the 18e sites by both sodium and aluminium atoms (Table 2). The resulting site occupancy would involve an average oxidation state $V^{+1.98}$. It has been reported that the sodiation capacity of NVP can be up to $Na_5V_2(PO_4)_3$ [41]. The crystallographic structure of ANVP is drawn in Fig. 6.

In contrast to the preservation of the NASICON-type structure, Wu et al. found very recently that the intercalation of Al^{3+} into V_2O_5 nanowires leads to the irreversible formation of an amorphous layer on the edge of nanowires and formation of a new crystalline phase [42]. Compared to V_2O_5 and other non-carbonaceous host materials [1,3,8-12, 42], it seems that the structure of NVP is more stable and suitable for aluminium insertion, although it is a slow process and the electrolyte solution should be optimized.

3.3. Electrochemistry in non-aqueous cell.

The selected electrochemical result using NVP in Al cell with ionic liquid as electrolyte solution (Fig.8) show a flat and reversible plateau at ca. 1.25 V vs. Al, and the reversible capacity is about 60-70 mAh g^{-1}. This plateau could be particularly suitable for developing Al batteries with a stable output voltage. These electrochemical results are very similar to those reported by Sun et al. [23], who proposed using $NaAlCl_4$ dissolved in EMIC. The mechanism of (de)intercalation could involve Al^{3+}, $AlCl_4^-$ and/or Na^+. In our case, the solution initially is sodium-free, but it is expected that after the first charge, a hybrid aluminium-sodium electrolyte be *in-situ* formed. Taking into account the size of the channels in NVP [26] and the size of $AlCl_4^-$ [17], intercalation of chloroaluminate ion is not expected. Our results agree well with those of Sun et al. [23], and sodium would be reversibly inserted in the case of using EMIC ionic liquid. However, having in mind our results using aqueous electrolyte, it could be possible to develop electrolytes compatible with both Al metal and aluminium ion insertion. An advantage could be a more rapid diffusion of smaller Al^{3+} compared to larger ions, such as sodium and lithium. Similarly, we have recently shown that the electrolyte also influences on the (de)insertion of magnesium in NVP [34].

4. Conclusions

Although Al-ion batteries are not yet competitive against lithium batteries, new possibilities have been studied here. We have proposed $Na_3V_2(PO_4)_3$ with NASICON-type structure as a new material for rechargeable aluminium batteries. Looking at the whole of all the results, it can be concluded that aluminium ions are effectively inserted in the framework of NVP using aqueous electrolyte, although some contribution of proton insertion cannot be completely excluded. A drawback would be the slow kinetics of the true insertion process, and at high charge/discharge rate the reaction is rather a pseudocapacitive process in the surface of NVP. Further efforts should be made to improve the cycling stability of this system. These finds suggest that after improving non-aqueous electrolyte that be compatible with both Al and NVP, new rechargeable batteries could be developed. This electrode material also can be used in non-aqueous cell vs. Al metal, with ionic liquid as electrolyte solution, in good agreement with the results of Sun et al. [23].

Acknowledgements

The authors are grateful to MINECO (grant number MAT2014-56470-R), FEDER funds and Junta de Andalucía (research group FQM288) for financial support. SCAI-UCO and Institute of Fine Chemistry and Nanochemistry are also thanked for facilitating the use of several instruments. The authors thank the help of M.J. Aragón with the synthesis.

References

1 Z. Rong, R. Malik, P. Canepa, G.S. Gautam, M. Liu, A. Jain, K. Persson, G. Ceder, Chem. Mater. 27 (2015) 6016.

2 G.A. Elia, K. Marquardt, K. Hoeppner, S. Fantini, R. Lin, E. Knipping, W. Peters, J.F. Drillet, S. Passerini. Adv. Mater. 28 (2016)7564.

3 J. R. González, F. Nacimiento, M. Cabello, R. Alcántara, P. Lavela, J. L. Tirado. RSC Adv. 6 (2016) 62157.

4 S. Liu, J. J. Hu, N. F. Yan, G. L. Pan, G. R. Li, X. P. Gao. Energy Environ. Sci. 5 (2012) 9743.

5 R. Chen, R. Luo, Y. Huang, F. Wu, L. Li. Adv. Sci. 3 (2016) 1600051.

6 Z.A. Zafar, S. Imtiaz, R. Razaq, S. Ji, T. Huan, Z. Zhang, Y. Huang, J.A. Anderson. Energy Environ. Sci. 5 (2017) 5646.

7 Q. Li, N.J. Bjerrum. J. Power Sources 110 (2002) 1.

8 M. Chiku, H. Takeda, S. Matsumura, E. Higuchi, H. Inoue. ACS Appl. Mater. Interfaces 7 (2015) 24385.

9 W. Wang, B. Jiang, W. Xiong, H. Sun, Z. Lin, L. Hu, J. Tu, J. Hou, H. Zhu, S. Jiao. Scientific Reports 3 (2013) 3383.

10 N. Jayaprakash, S. K. Das, L. A. Archer. Chem. Commun. 47 (2011) 12610.

11 S. Gu, H. Wang, C. Wu, Y. Bai, H. Li, F. Wu. Energy Storage Materials 6 (2017) 9.

12 Y. J. He, J.F. Peng, W. Chu, Y.Z. Li, D.G. Tong. J. Mater. Chem. A 2 (2014) 1721.

13 B. Lee, H.R. Lee, T. Yim, J.H. Kim, J.G. Lee, K.Y. Chung, B. W. Cho, S. H. Oh. J. Electrochem. Soc. 163 2016) A1071.

14 N.S. Hudak. J. Phys. Chem. C 118 (2014) 5203.

15 S. Liu, G. L. Pan, G. R. Li, X. P. Gao. J. Mater. Chem. A 3 (2015) 959.

16 M.C. Lin, M. Gong, B. Lu, Y. Wu, D.Y. Wang, M. Guan, M. Angell, C. Chen, J. Yang, B.J. Hwang, H. Dai. Nature 520 (2015) 324.

17 S. C. Jung, Y.J. Kang, Y.K. Han. Electrochim. Acta 223 (2017) 135.

18 K.V. Kravchyk, S. Wang, L. Piveteau, M.V. Kovalenko. Chem. Mater. 29 (2017) 4484.

19 C. Masquelier, L. Crogennec. Chem Rev. 113 (2013) 6552.

20 R. Klee, M. Wiatrowski, M.J. Aragón, P. Lavela, G. F. Ortiz, R. Alcántara, J.L. Tirado. ACS Appl. Mater. Interfaces 9 (2017) 1471 .

21 G. Li, Z. Yang, Y. Jiang, C. Jin, W. Huang, X. Ding, Y. Huang. Nano Energy 25 (2016) 211.

22 V. Palomares, P. Serras, I. Villaluenga, K.B. Hueso, J. Carretero-González, T. Rojo. Energy Environ. Sci. 5 (2012) 5884.

23 X. Sun, Z. Zhang, H. Guan, C. A. Bridges, Y. Fang, Y. Hu, G. M. Veith, S. Dai. J. Mater. Chem. A 5 (2017).

24 J. Y. Luo, W. J. Cui, P. He, Y. Y. Xia. Nat. Chem. 2 (2010) 760.

25 W.X Song, X.B. Ji, Y.R Zhu, H.J Zhu, F.Q Li, J. Chen, F. Lu, Y.P Yao, C.E. Banks. ChemElectroChem 1 (2014) 871.

26 H. Zhou, Z.R. Tian, S.S. Ang. Mater Renew Sustain Energy (2016) 5:3.

27 C.W. Mason, F. Lange. ECS Electrochem. Lett. 4 (2015) A79.

28 L. Zhang, T. Huang, A. Yu. J. Alloy Compd. 646 (2015) 522.

29 Q. Zhang, C. Liao, T. Zhai, H. Li. Electrochim. Acta 196 (2016) 470.

30 G. Li, Z. Yang, Y. Jiang, W. Zhang, Y. Huang. J. Power Sources 308 (2016) 52.

31 G. Li, Z. Yang, Y. Jiang, C. Jin, W. Huang, X. Ding, Y. Huang. Nano Energy 25 (2016) 211.

32 P.R. Kumar, Y.H. Jung, C.H. Lim, D.K. Kim. J. Mater. Chem. A 3 (2015) 6271.

33 H. B. Zhao, C. J. Hu, H. W. Cheng, J. H. Fang, Y. P. Xie, W. Y. Fang, T. N. L. Doan, T. K. A. Hoang, J. Q. Xu, P. Chen. Scientific Reports 6 (2016) 25809.

34 M. Cabello, R. Alcántara, F. Nacimiento, P. Lavela, M.J. Aragón, J.L. Tirado. Electrochim. Acta 246 (2017) 908.

35 K. Momma, F. Izumi. J. Appl. Crystallogr. 44 (2011) 1272.

36 R.N. Reddy, R.G. Reddy. J. Power Sources 156 (2006) 700.

37 H. Lindström, S. Sö1dergren, A. Solbrand, H. Rensmo, J. Hjelm, A. Hagfeldt, S.E. Lindquist. J. Phys. Chem. B 101 (1997) 7717.

38 Z. Jian, C. Yuan, W. Han, X. Lu, L. Gu, X. Xi, Y.S. Hu, H. Li, W. Chen, D. Chen, Y. Ikuhara, L. Chen. Adv. Funct. Mater. 24 (2014) 4265.

39 W.X. Song, X.Y. Cao, Z.P. Wu, J. Chen. Phys. Chem. Chem. Phys. 16 (2014) 6845.

40 M.J. Aragón, J. Gutiérrez, R. Klee, P. Lavela, R. Alcántara, J.L. Tirado. J. Electroanal. Chem. 47 (2017) 47.

41 Z. Jian, Y. Sun., X. Ji. Chem. Commun. 51 (2015) 6381.

42 S. Gu, H. Wang, C. Wu, Y. Bai, H. Li, F. Wu. Energy Storage Mater. 6 (2017) 9.

Table 1. Compositions and lattice cell parameters of NVP and ANVP electrode materials. The given theoretical compositions were calculated by assuming that all the electrons that flow through the electrochemical cell are employed to the assumed (de)insertion reaction (coulometric measurement). The experimental compositions were obtained by EPMA.

NVP electrode	**Theoretical composition**	**Experimental composition**	**Lattice cell parameters, Å**
raw	$Na_3V_2(PO_4)_3$	$Na_{2.8}V_2(PO_4)_{3.5}$	a=8.735(5) c=21.82(1)
after first charge	$Na_{1.1}V_2(PO_4)_3$	$Al_{0.06}Na_{0.94}V_2(PO_4)_{2.6}$	a=8.401(1) c=21.444(4)
after charge+discharge	$Al_{0.3}Na_{1.1}V_2(PO_4)_3$	$Al_{0.25}Na_{0.81}V_2(PO_4)_{2.2}$	a=8.51(1) c=21.81(3)

Table 2. Crystallographic data for the ANVP electrode after-charge discharge of NVP in aluminum cell, obtained from Rietveld refinement. Space group: R-3c.

atom	Wyckoff site	x	y	z	occupancy
Na1	6b	0.0000	0.0000	0.0000	0.9753
Na2	18e	0.7745	0.0000	0.2500	0.2432
Al	18e	0.7522	0.0000	0.2500	0.4042
V	12c	0.0000	0.0000	0.1439	1.0000
P	18e	0.3068	0.0000	0.2500	1.0000
O1	36f	0.1700	-0.0074	0.2000	1.0000
O2	36f	0.1953	0.1637	0.1006	1.0000

FIGURE CAPTIONS

Figure 1. Selected CV results for NVP. (a) First and second scan in $AlCl_3$(aq) at 1.0 mV s^{-1}. (b) First scan in NaCl/HCl and HCl solutions at 1 mV s^{-1} (c) Second scan at several scan rates in $AlCl_3$(aq). (d) Peak intensity as a function of sweep rate in $AlCl_3$(aq).

Figure 2. Galvanostatic cycling of NVP in $AlCl_3$(aq). (a) Typical voltage-capacity curves at 10 mA g^{-1} of current density. (b) Capacity-cycle number at several rates (charge: open symbols, discharge: closed symbols).

Figure 3. SEM micrograph of ANVP electrode and mapping of composition for Na, Al and P, obatained after the first charge-discharge cycle of NVP and washing with deionized water.

Figure 4. ^{27}Al MAS NMR spectra for: (a) NVP after the first charge-discharge cycle (nominal composition $Al_{0.3}Na_{1.2}V_2(PO_4)_3$) and after washing to remove electrolyte, and (b) NVP electrode impregnated with electrolyte solution (no cycling, no washing).

Figure 5. XP spectra for pristine NVP and electrodes retrieved from the cells.

Figure 6. Ex situ XRD of NVP electrodes at selected states of charge in aqueous aluminum cell. The Miller indexes of the main reflections are given. The reflections from Ti current collector are marked.

Figure 7. Structural views of ANVP.

Figure 8. Galvanostatic results for NVP in non-aqueous cell. Current density: 3 mA g^{-1}.

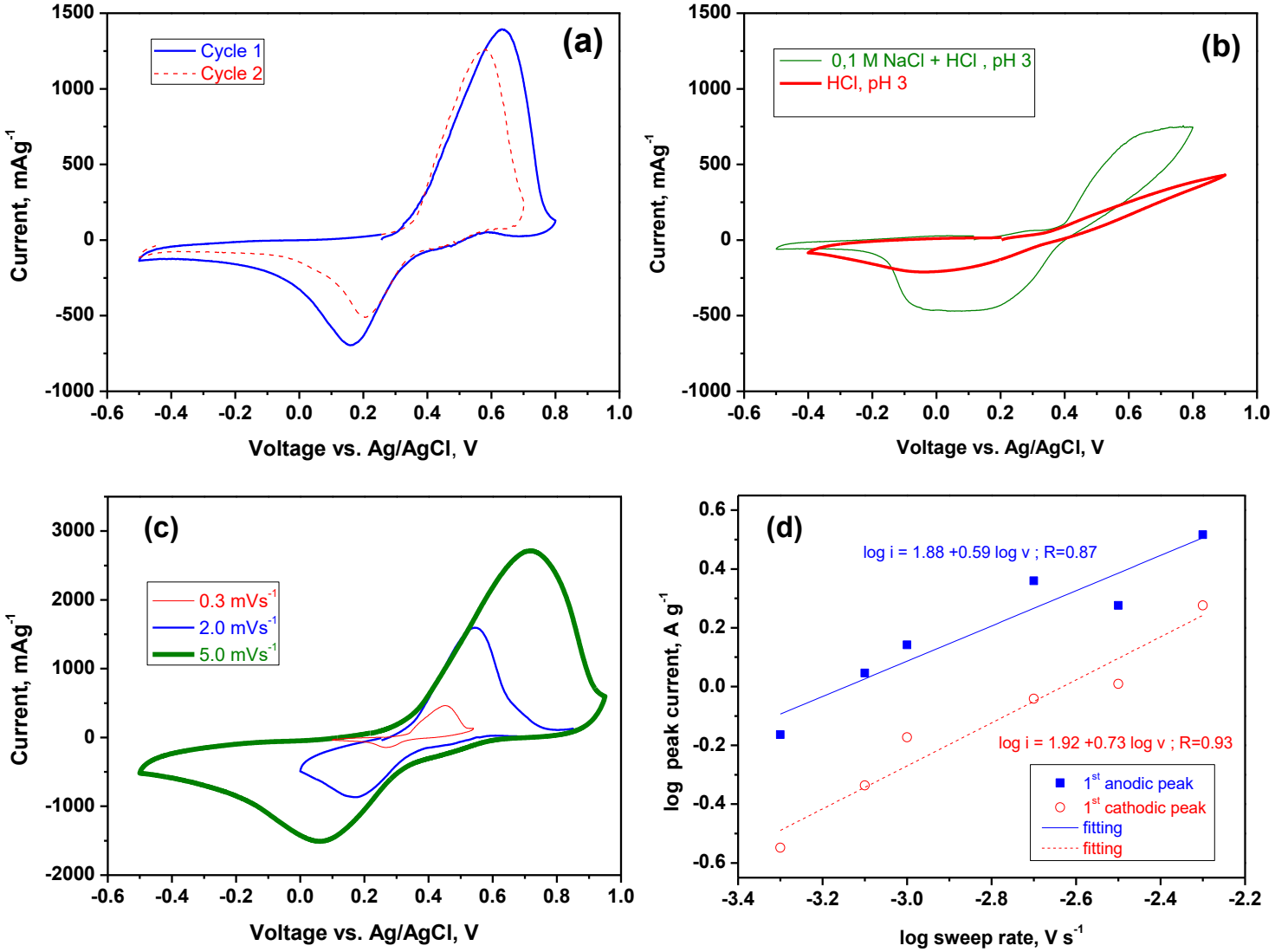
(a)
Cycle 1
Cycle 2
Current, mAg-1
Voltage vs. Ag/AgCl, V
(b)
0,1 M NaCl + HCl , pH 3
HCl, pH 3
Current, mAg-1
Voltage vs. Ag/AgCl, V
(c)
0.3 mVs-1
2.0 mVs-1
5.0 mVs-1
Current, mAg-1
Voltage vs. Ag/AgCl, V
(d)
log i = 1.88 +0.59 log v ; R=0.87
log i = 1.92 +0.73 log v ; R=0.93
1st anodic peak
1st cathodic peak
fitting
fitting
log peak current, A g-1
log sweep rate, V s-1

Figure 1.

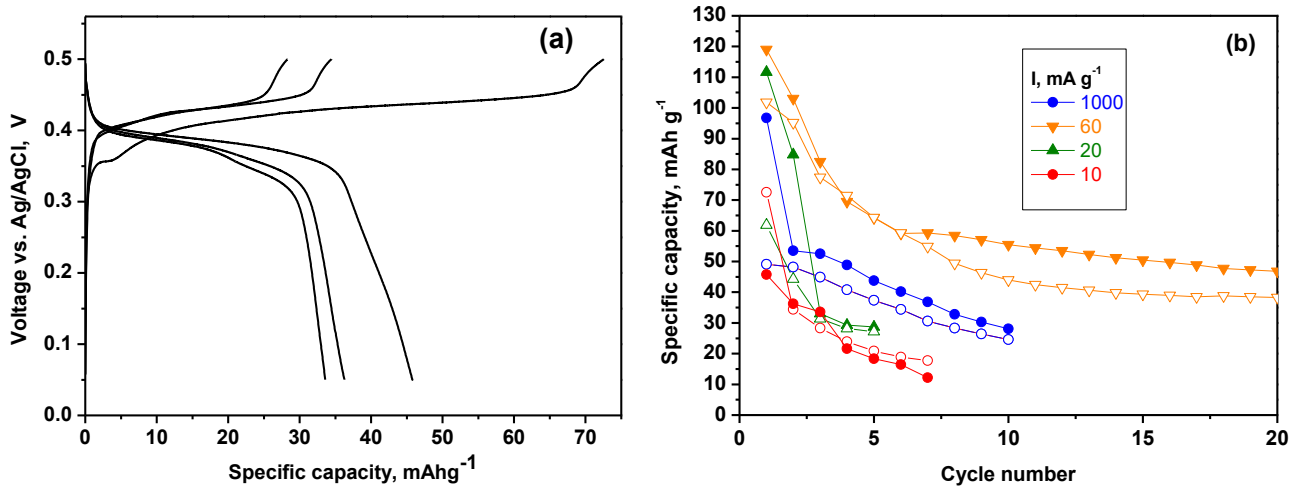
(a)
Voltage vs. Ag/AgCl, V
Specific capacity, mAhg-1
(b)
I, mA g-1
1000
60
20
10
Specific capacity, mAh g-1
Cycle number

Figure 2.

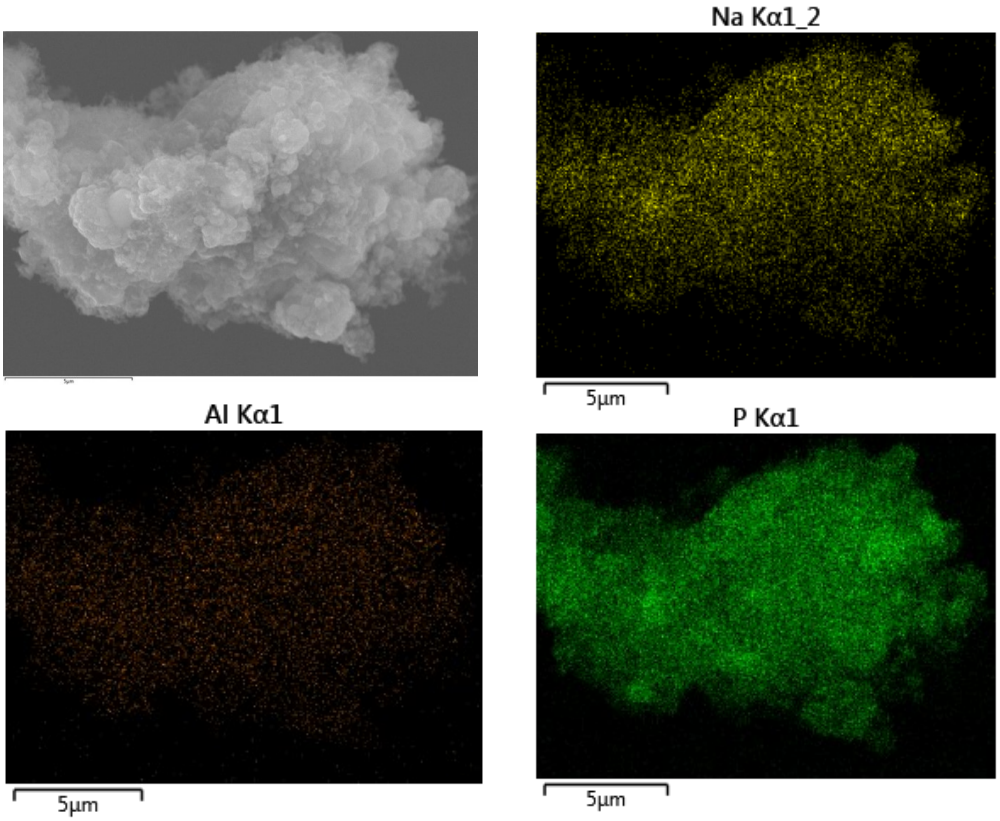

Figure 3.

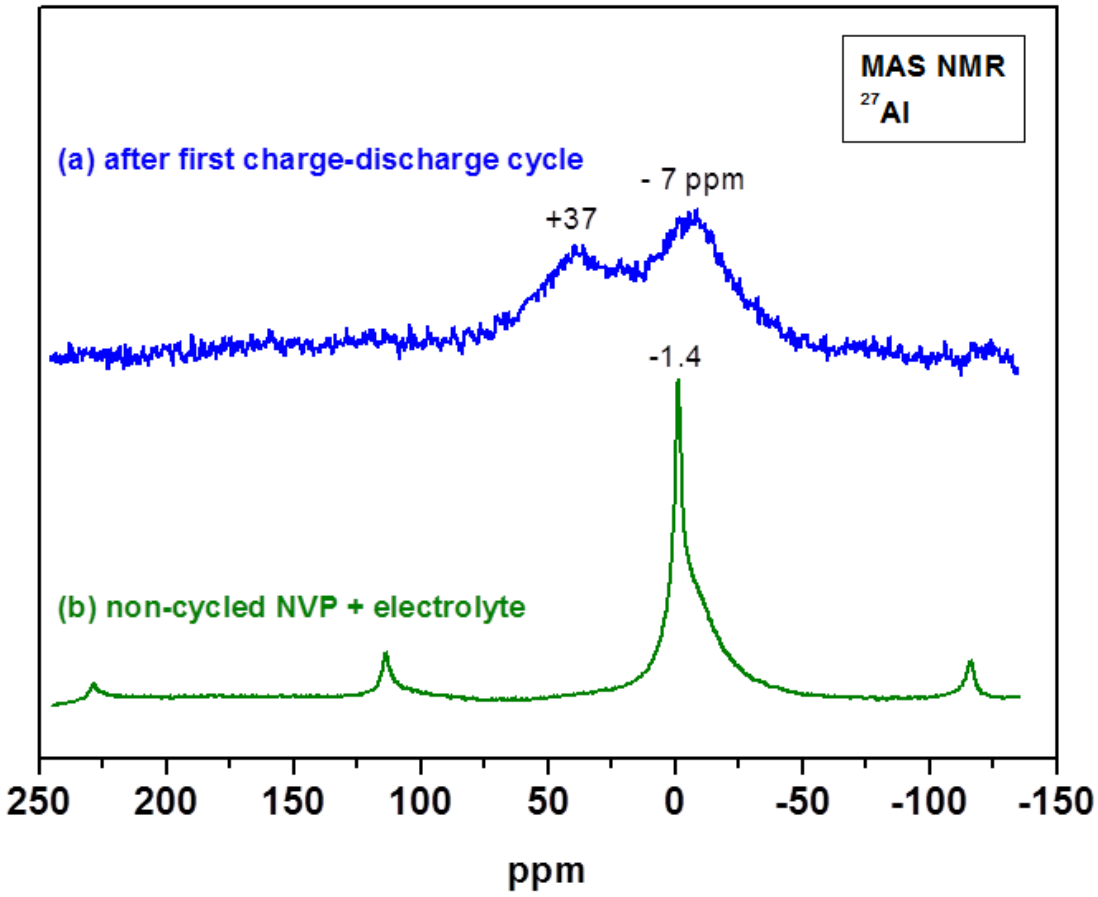
MAS NMR
27Al
(a) after first charge-discharge cycle
- 7 ppm
+37
-1.4
(b) non-cycled NVP + electrolyte
250
200
150
100
50
0
-50
-100
-150
ppm

Figure 4.

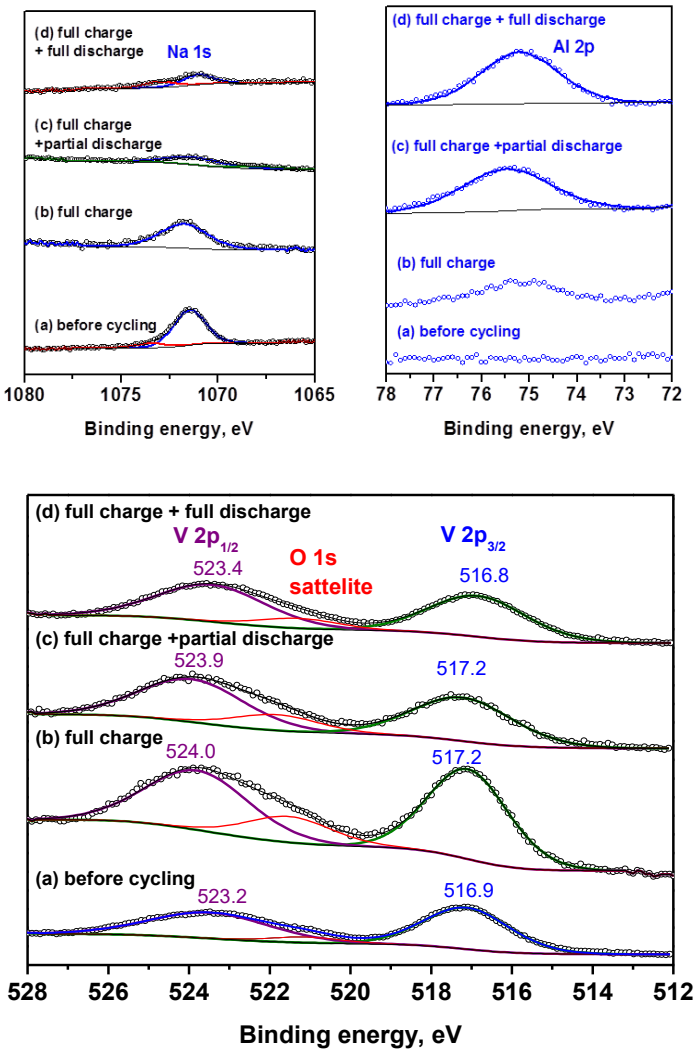
(d) full charge
+ full discharge
Na 1s
(c) full charge
+partial discharge
(b) full charge
(a) before cycling
1080
1075
1070
1065
Binding energy, eV
(d) full charge + full discharge
Al 2p
(c) full charge +partial discharge
(b) full charge
(a) before cycling
78
77
76
75
74
73
72
Binding energy, eV
(d) full charge + full discharge
V 2p1/2
523.4
O 1s
sattelite
V 2p3/2
516.8
(c) full charge +partial discharge
523.9
517.2
(b) full charge
524.0
517.2
(a) before cycling
523.2
516.9
528
526
524
522
520
518
516
514
512
Binding energy, eV

Figure 5.

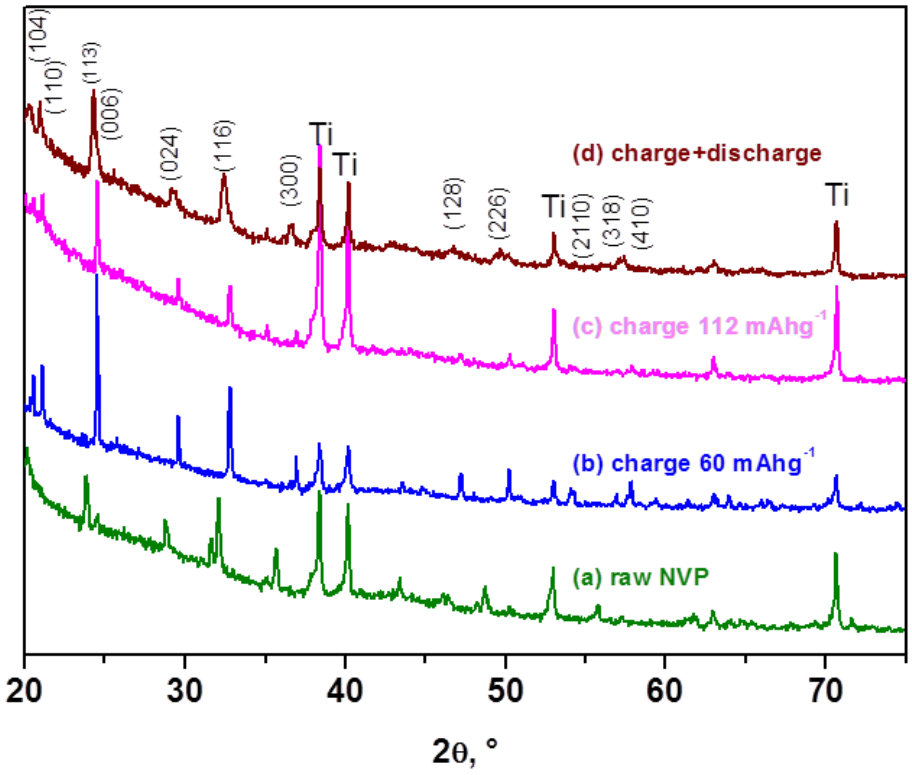
(104)
(110)
(113)
(006)
(024)
(116)
(300)
Ti
Ti
(128)
(226)
Ti
(2110)
(318)
(410)
Ti
(d) charge+discharge
(c) charge 112 mAhg-1
(b) charge 60 mAhg-1
(a) raw NVP
20
30
40
50
60
70
2θ, °

Figure 6.

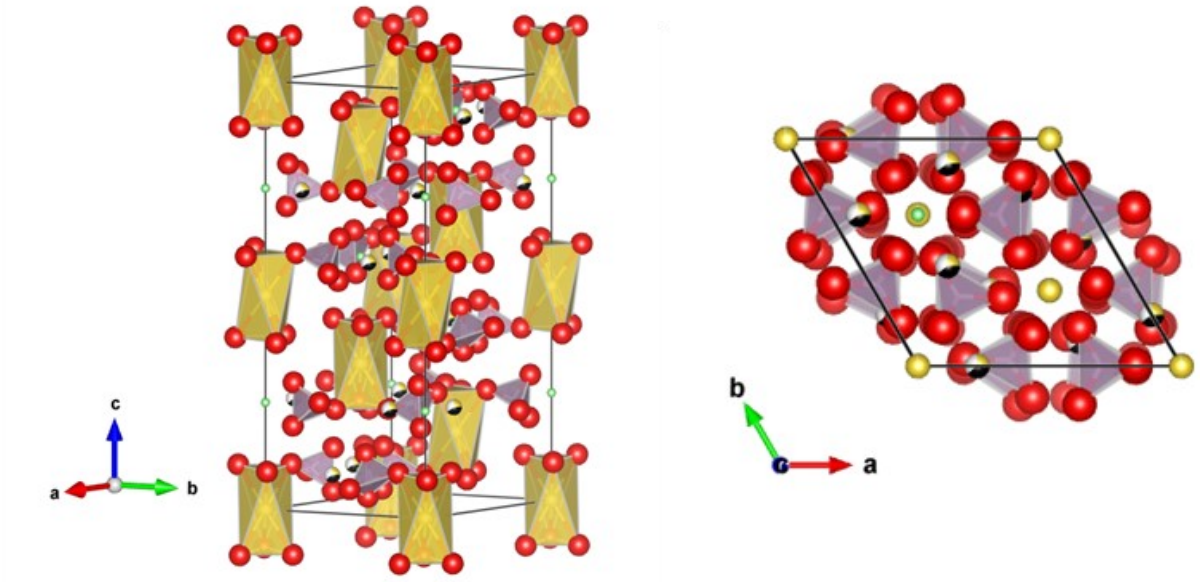

Figure 7.

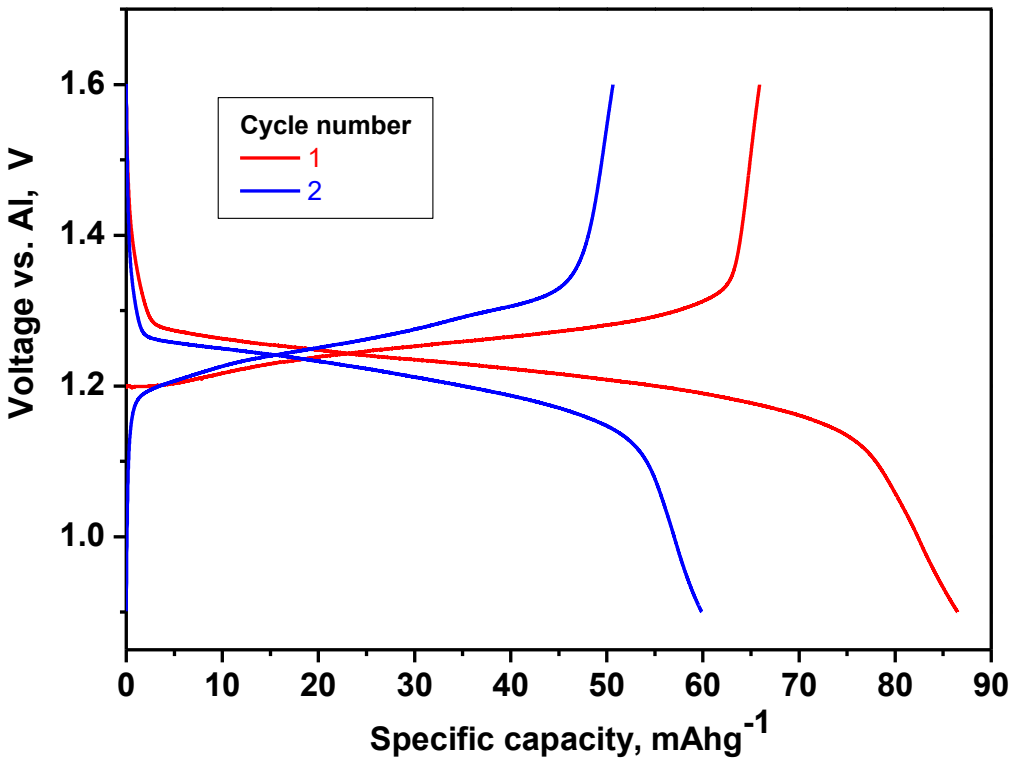
Cycle number
1
2
Voltage vs. Al, V
1.6
1.4
1.2
1.0
0
10
20
30
40
50
60
70
80
90
Specific capacity, mAhg-1

Figure 8.